Volume 1 | Number 1 | Jan 2013 | Pages 1–100

Journal of
Materials Chemistry A

Materials for energy and sustainability
www.rsc.org/materialsA

Li⁺

ROYAL SOCIETY
OF CHEMISTRY

ROYAL SOCIETY
OF CHEMISTRY

www.rsc.org/materialsA

Journal of Materials Chemistry A

Insight into the Electrochemical Activation of Carbon-Based Cathodes for Hydrogen Evolution Reaction

Guofa Dong[‡,a,b], **Ming Fang**[‡,a,b], **Hongtao Wang**[c], **Senpo Yip**[a,b], **Ho-Yuen Cheung**[d], **Fengyun Wang**[e], **Chun-Yuen Wong**[d], **Saitak Chu**[*,a] **and Johnny C. Ho**[*,a,b]

Recently, carbon nanomaterials have been reported with the outstanding electrocatalytic performance for hydrogen evolution reaction (HER) after electrochemical activation;
10 **however, the exact activation mechanism is still under extensive debate. In this work, for better understanding the activation, graphite rod and carbon nanohorns, two typical carbon materials in different scales, were electrochemically activated and their catalytic performance on HER was also**
15 **systematically studied, which showed that the HER performance was greatly affected by the counter electrode employed for the activation. An efficient activation was achieved when a platinum wire was used as the counter electrode and, simultaneously, the Pt transfer from the anode**
20 **to the cathode was also observed. All these suggest that the improved HER performance was mainly caused by the Pt transfer, rather than the activation of carbon materials themselves. More importantly, our study implied that the Pt dissolution, although being widely ignored, should be taken**
25 **into reconsiderations during electrochemical tests when Pt metal is utilized as the counter electrode.**

1. Introduction

Due to its superior efficiency, zero pollution and good recyclability, hydrogen has been considered as one of the
30 most promising alternative fuels for tackling the problems of energy crisis as well as environmental pollution in future[1, 2]. In general, electrolysis of water, an important method for the hydrogen production, has been employed in various industrial processing sectors for decades and recently
35 attracts more and more interests for energy applications. However, owing to the obstacle from overpotential, the required potential in water electrolysis is always much higher than the standard value, which inevitably leads to a huge waste of power[3, 4]. In order to improve the efficiency of
40 water electrolysis, noble metal catalysts such as Pt, Pd, Ru, or their alloys are often adopted and integrated into the electrodes to lower the overpotential because of their excellent electrocatalytic performance on the hydrogen evolution reaction (HER)[5, 6]. On the contrary, these noble

45 metals are not only expensive, but also scarce with limited reserve on the earth; as a result, all these noble catalysts are far from sustaining the future development of hydrogen evolution. In this regard, developing novel and low-cost catalysts with high catalytic performance for HER is an
50 imperative task in the research of electrochemical water splitting[7, 8].

In the past few years, many promising non-noble electrocatalysts, including transition metal sulfides, selenides, borides, carbides, nitrides and phosphides, have
55 been extensively exploited for HER[5, 9, 10]. Nevertheless, achieving efficient catalysts with the high activity and good stability for HER is still a big challenge. Until recently, carbon nanomaterials such as carbon nanotubes and fullerenol were reported with the outstanding catalytic
60 performance on HER after electrochemical activation[11-13]. Especially, the activated single-walled carbon nanotube film exhibited remarkable electrocatalytic performance almost as good as that of platinum on HER[13]. Some researchers also proposed the mechanism of this activation and attributed
65 these performance improvements to the increase of the number of oxygen functionalities which was considered as the active sites for HER, or the "adjacent Tafel" mechanism[11-13], but the exact mechanism is still unclear. In some previous studies, carbon materials just surprisingly gave the poor
70 catalytic activity on HER[14] and often used as structural scaffolds for catalysts[7, 15-17]. In this work, in order to obtain a better and clear understanding for this activation, pure graphite rods were utilized as the working electrode and electrochemically activated. It was found that the type of
75 counter electrode employed for the activation could fundamentally determine the HER performance of the working electrodes after activations. When a Pt wire was used as the counter electrode, the working electrode could be effectively activated after 13000 cyclic voltammetry (CV)
80 cycles and yielded the extraordinary catalytic performance for HER. However, with a graphite rod as the counter electrode, even increasing the activation to 15000 CV cycles or after a potentiostatic treatment of 20000 s, there was almost no improvement there. Further characterization by
85 SEM, TEM and XPS verified that when the counter electrode

was a Pt wire, Pt nanoparticles would form on the working electrode and actually led to the improved electrocatalysis on HER. Carbon nanohorns, as a metal-free nano-sized carbon material[18,19], was also treated with the same activation procedure and similar results as those on the graphite rods were obtained. All these would imply that the anodic platinum dissolution and subsequent transfer during the potential scan cycles must be responsible for the formation of Pt nanoparticles on the cathode. We hereby suggest that CV cycling is not a valid method for activating carbon materials into efficient HER catalysts and metal contamination should be taken into considerations during electrochemical tests when Pt is used as the counter electrode.

2. Experimental

2.1 Materials

Isopropyl alcohol (99.7%), sulphuric acid (H_2SO_4, >95%) and Nafion@solution (5% in a mixture of lower aliphatic alcohols and water) were purchased from Sigma-Aldrich. All chemicals were used as received without further purification. Pure graphite rods (8 mm in diameter, 99.999% purity with trace metals basis) were obtained from Shanghai New Graphite Material CO., LTD. The commercial Pt/C powder (20 wt % Pt on Vulcan XC-72) was purchased from Alfa Aesar. The platinum wire is commercially available and with a purity of 99.99 w%. All the water used throughout the experiments was purified through a Millipore system.

2.2 Fabrication of the working electrode

In order to exclude the interference from metal elements at the greatest extent, highly pure graphite rods were used as the working electrodes or counter electrode. Here, the working electrodes were fabricated with the following processes. The graphite rods were first cut into a length of ~ 3 cm. Next, the cross section of graphite electrode were polished with SiC abrasive paper (Eagle, 1500 type) and weighing paper consecutively, and then washed ultrasonically with water for twice to get rid of the remained graphite powder. Finally, the column parts of the working electrodes were sealed with water-proof tape and only the smooth cross section was exposed as the reactive interface for the experiment. It is noted that two graphite working electrodes were newly fabricated and used separately for the activations with different counter electrodes.

2.3 Preparation of carbon nanohorns

Carbon nanohorns (CNHs) were prepared by a modified arc discharge method reported in the literature[19]. Typically, two highly pure graphite rods with a diameter of 8 mm reacted under a DC arc-discharge in a water-cooled stainless steel chamber filled with 400 Torr of air as the buffer gas. The discharge current was kept at about 140 A. As the anode was consumed, the distance between two electrodes was maintained at a constant value of about 1 mm. After the discharge, the chamber was cooled down to room temperature and opened. Then the soot on the inner and upper wall of the reaction chamber was collected for further use.

2.4 Instrumentation and measurements

The scanning electron microscopy (SEM) images were taken on a Phenom Pro SEM (FEI, US) and a Hitachi, SU-70 SEM system (Hitachi, Japan). The transmission electron microscopy (TEM) and HR-TEM images were obtained by a Tecnai G2 F20 S-TWIN (FEI, US) field emission electron microscope and the acceleration voltage was 200 kV. The high-angle annular dark-field scanning transmission electron microscopy (HAADF-STEM) and corresponding energy-dispersive X-ray spectroscopy (EDS) mapping analysis were performed on a Titan G2 80-200 TEM/ChemiSTEM (FEI, US) with a spherical aberration corrector. X-ray photoelectron spectra (XPS) were acquired on an ESCALAB 250 XPS system. Before all the measurements, the electrode surface were washed with DI water for several times and dried at 50 ^{o}C in open air. For the TEM observation, a thin surface layer of the electrode was gently scratched off from the working area and ultrasonically dispersed in absolute ethanol. Then a droplet of the above dispersion was dropped on the copper micro-grid coated with holey carbon and dried in open air. The purity of Pt wire was determined on an Environmental Scanning Electron Microscope (FEI / Philips XL30 ESEM-FEG) system before the electrochemical activation and the corresponding details are shown in Electronic Supplementary Information (ESI).

2.5 Electrochemical measurements

A standard electrochemical cell with three electrodes was set up for all the electrochemical activations and electrochemical tests. A Pt wire or a graphite rod was used as the counter electrode and a saturated calomel electrode (SCE) was used as the reference electrode. All electrochemical activation and determination were performed on a G300 workstation (Gamry Instruments, USA). Here for simplicity, we denote the working graphite electrodes as Pt-GE and G-GE, respectively, when the Pt wire or graphite rod was used as the counter electrode for activation. The electrochemical activations were carried out by CV scan in a potential range from -0.56 V to +0.24 V with a scan rate of 50 mVs^{-1}. The electrocatalytic activities towards HER were determined by linear sweep voltammetry (LSV) with a scan rate of 5 mVs^{-1}. For the purpose of comparison, the catalytic performance of the commercial Pt/C powder (20 wt % Pt on Vulcan XC-72) was also measured under similar conditions by loading it on a glassy carbon working electrode (GCE).The Pt/C powder was loaded by the drop casting method and the details can be found in ESI. The catalytic activity of CNH for HER was also determined by the same procedure exploited on Pt/C powder. All the electrochemical activations or examinations were carried out at room temperature in 0.5 M H_2SO_4 solution. For every electrochemical experiment, the cell was first washed with DI water and then rinsed with 0.5 M H_2SO_4 solution before the new electrolyte was added in. All the potentials reported in this work were referred to a reversible hydrogen electrode (RHE) by adding a value of (0.242 +

0.059×pH) V and all the LSV curves were corrected through the iR compensation to eliminate the error from the internal resistance. All the current density values were determined based on the geometric area of the electrode.

3. Results and discussion

3.1 The electrocatalytic activity on HER

As mentioned above, the working graphite rods were activated by continuous potential scan with different counter electrodes. Then, the corresponding LSV curves were recorded in order to investigate their electrocatalytic activity on HER. Fig. 1 demonstrates all the polarization curves measured from different graphite rods. It is clear that before any activation, the graphite rods showed a substantial overpotential of more than 500 mV whenever either a Pt wire or a graphite rod was utilized as the counter rod. When a graphite rod was used as the counter electrode, there was not any apparent improvement on the HER electrocatalytic activity even after 15000 CV activation cycles (Fig. 1b). The onset potential for HER was still at about -480 mV and the corresponding current density was just about 0.7 mA cm^{-2}, which indicated the G-GE was failed to be activated. However, when a Pt wire was employed as the counter electrode and after 13000 CV cycles of activation, the HER overpotential was sharply decreased to 20 mV while the corresponding current density was still kept at ~10.4 mA cm^{-2} (Fig 1a). These values were very close to those determined on the commercial Pt/C. Obviously, the graphite rod was effectively activated after the pre-treatment with a Pt wire as the counter electrode. All these explicitly indicate that the type of counter electrodes exploited for the activation plays a decisive role in the HER activity of the activated working graphite rod.
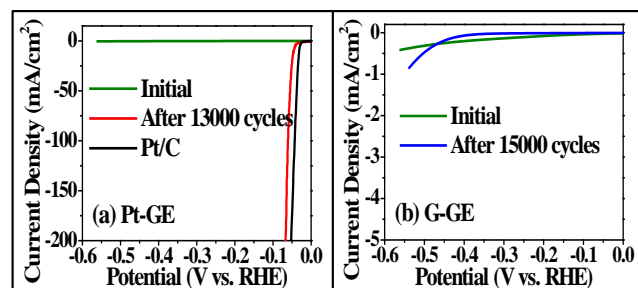
Fig.1 LSV curves on HER of graphite rods activated with different counter electrodes: (a) curves recorded before and after 13000 CV cycles' activation when using a Pt wire as counter electrode. The black line is the HER curve on commercial Pt/C for comparison; (b) curves collected before and after the activation of 15000 CV cycles when a graphite rod is used as counter electrode.

3.2 Functional details of counter electrodes

Since all electrode reactions are essentially the interfacial processes occurred between the solid surface of the electrode and the adjacent thin layer of the solution, the surface properties of electrodes play a crucial role on these interfacial reactions. Many factors such as the chemical composition, structure, morphology and electrical properties of the electrode surface would fundamentally determine the possibility, direction and reactive rate of the electrode

reactions; therefore, the working graphite rod was thoroughly examined by SEM, TEM, XPS and EDS mapping in order to further understand the functional details of counter electrodes during the activation process.

Surface morphologies

Fig. 2 depicts all the SEM images of the graphite rod surfaces. As shown in Fig. 2a, it is evident that before any activation, the initial surface of the graphite electrode was very rough and disorder, full of graphite flakes or particles, although it looked very flat and smooth by naked eyes. However, after 13000 CV activation cycles, many tiny and shiny particles could be observed in Fig. 2b, dispersing densely on the surface of Pt-GE when using a Pt wire as the counter electrode. The magnified SEM and TEM pictures (Fig. 2b inset and Fig. 3a, b) further illustrated that the size of these particles was less than 100 nm and the shapes of the particles were irregular. Completely different from the surface on the Pt-GE, when a graphite rod was used as the counter electrode even after 15000 CV cycles of activation, there was not any similar particle but only loose graphite layers observed on the surface of G-GE (Fig. 2c). Based on the significant difference of surface morphology and electrochemical properties of Pt-GE and G-GE after different activations, those nanoparticles should be responsible for the greatly elevated HER activity on Pt-GE and the use of Pt counter electrode must be the decisive factor to the generation of these particles; as a result, the elemental analysis of these particles can give further useful information on the mechanism of the electrode activation here.
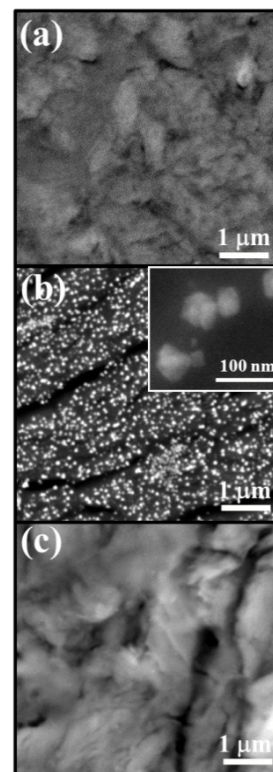
Fig.2 SEM images of (a) the initial graphite electrode surface, (b) the graphite electrode surface after 13000 CV activation cycles when using a Pt wire as the counter electrode and (c) the graphite electrode surface after

15000 CV activation cycles with a graphite rod used as the counter electrode. The inset in (b) is the magnified picture of the Pt nanoparticles.

Elemental analysis

The EDS spectra depicted in ESI Fig. S1 shows that the commercial Pt wire is highly pure in quality while as shown in ESI Fig. S2, the initial graphite electrode surface mainly consisted of carbon (~96.5 atom %) and oxygen (~3.5 atom %). After the activation of 13000 CV cycles, the corresponding EDS mapping (Fig. 3) revealed that the elements distributed on the surface of Pt-GE are mostly platinum, carbon and oxygen. A detailed EDS analysis can also be found in ESI Fig. S3. The signal of S and O can be derived from the absorption of SO_4^{2-} into the background graphite layers of the Pt-GE. All these clearly suggest that the tiny and shiny nanoparticles are platinum related species on the surface of Pt-GE after the activation.

At the same time, XPS was also employed to study the chemical composition of the electrode surface. It is clear that when a Pt wire was used as the counter electrode before the activation, there were just peaks of C1s and O1s with the binding energy of 284.6 eV and 531.9 eV[20-22], respectively. After the activation, in addition to C $1s$ and O $1s$ peaks, characteristic peaks of Pt $4f_{7/2}$, Pt $4f_{5/2}$, Pt $4d_{5/2}$ and Pt $4d_{3/2}$ were also present at 71.2 eV, 74.4 eV, 314.2 eV and 332.1 eV, accordingly[22-25]. Consistent with the previous reports[23, 26, 27], if there were oxygen atoms absorbed or chemically bonded on the Pt particles, Pt $4f$ should reveal a shoulder on the high binding energy side of the Pt $4f_{5/2}$ peak at a binding energy of ~76.5 eV; however, there was not such a peak in the Pt $4f$ spectra, indicating that the nanoparticles formed on the surface of Pt-GE are pure metallic Pt particles. It should also be noted that the weak peak at 169.2eV can be attributed to S $2p_{3/2}$, which corresponds to the +6 oxidation state of sulfur and demonstrates the existence of SO_4^{2-} in the electrode surface layers. In any case, the XPS results further confirmed the existence of metallic Pt nanoparticles and sulfate ions on the activated electrode surface, which was in accordance with the results from TEM observation.
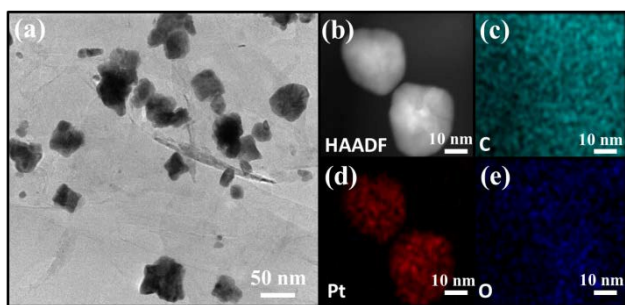
Fig.3 TEM image and the elemental mapping of the graphite electrode surface after an activation of 13000 CV cycles when using a Pt wire as counter electrode. (b-e) HAADF-STEM image and corresponding EDS mapping of the Pt particles, indicating the distribution of C, Pt and O, respectively.
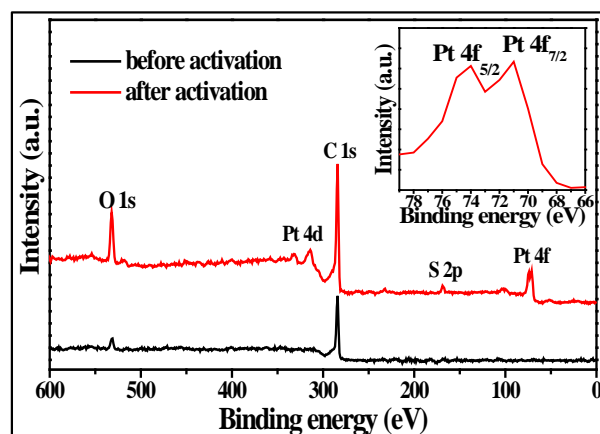
Fig.4 XPS spectra of the graphite rod before and after an activation of 13000 CV cycles when using a Pt wire as the counter electrode.

3.3 The formation process of Pt particles

Monitoring the activating process as well as understanding the formation process of Pt particles is very important in investigating the transformation process of the working electrode surface during the activation period. Here, the LSV curves on HER were determined and SEM pictures were taken as well after different activating CV cycles (ESI Fig. S4-5). As depicted in Fig. S4a, the onset potential for HER on Pt-GE became smaller with the increasing CV cycles while the corresponding current density went higher and higher at the same time. At the initial 10000 cycles, the variation of the onset potential and current density was relatively slow. On the other hand, from 10000 to 12000 cycles, there was a distinct improvement on the HER activity. These changes are found to have a direct relation with the variation of the electrode surface. ESI Fig. S5 gives the electrode surface evolution of Pt-GE during the activation period. At the beginning, there were full of graphite flakes or particles on the surface (Fig. S5a and f). After 4000 CV cycles, some tiny bright nanoparticles began to appear (Fig. S5b and g). From then till 12000 CV cycles, more particles were explicitly formed, densely and uniformly dispersed on the electrode surface (Fig. S5c-e and h-j). Since the highly pure graphite rod (99.999%) was employed as the working electrode during the activation of Pt-GE, the Pt wire is apparently the only source of Pt and somehow these Pt got transferred from the anode to the cathode, leading to the generation of these Pt nanoparticles as shown in Fig. 3. In specific, Pt was first dissolved from the wire into the H_2SO_4 solution along with the CV scan. The dissolved Pt species (Pt^{2+} or PtO_x) then dispersed into solution[28-30], and got reduced into Pt atoms and regenerated on the cathode surface. The dissolution of Pt is a slow process as the rate determining step; as result, at the initial thousands of CV cycles the concentration of Pt species was relatively low and just a few Pt atoms could be regenerated. With the increasing cycles, the concentration of Pt species became eventually higher. According to Le Chatelier's Theory, a higher concentration of Pt species would greatly increase the productivity of Pt atoms on the cathode, and thus more Pt particles would get formed onto the cathode surface, which largely enhanced the

corresponding electrochemical performance for HER.

3.4 Possible dissolution mechanism of Pt wire

The dissolution of platinum is an important research topic which is often studied in the area of polymer electrolyte fuel
[5] cells (PEFCs)[30-33], since the dissolution not only washes away Pt from the electrode but also deteriorates the overall performance of PEFCs[34, 35]. Many experimental factors such as temperature, scan rate, as well as variation mode and range of the potential scan will greatly affect the dissolution
[10] rate of Pt[33, 36-40]. Matsumoto and Akihiko have found that the existence of oxygen can also increase the dissolution rate and the amount of Pt dissolved in acidic environments[37, 39]. Although there have been lots of reports on the Pt dissolution, the exact mechanism is still ambiguous. Most
[15] researchers have paid much attention to the cathode dissolution of Pt in the high potential range only which is mainly related to the applications of oxygen reduction reaction or oxidation of fuels[29, 31, 33, 35]. To the best of our knowledge, there are few reports on anodic dissolution of Pt
[20] in low potential range during the HER process. Based on the previous studies on the dissolution mechanism of Pt[30, 37, 39, 41], the Pt oxide layer was first formed and then dissolved under the function of potential scan. During the HER process in low potential range, different oxygen species such as atomic
[25] oxygen (O), peroxide radical ($\cdot HO_2$) and O_2 will be generated extensively on the anode[42], which will heavily influence the dissolution progress of Pt. The possible scheme of dissolution of Pt in this work is proposed in Fig. 5. At the first step, H_2O or OH^- was absorbed on Pt surface. In the
[30] second step, these absorbed species were oxidized into the following products: oxygen atom, $\cdot HO_2$ or O_2 in which the former two are strong oxidizing agents and they would react with Pt instantly after their evolution. This way, the Pt metal would soon be covered with an oxide layer or become Pt^{2+}
[35] ions. Some oxygen atoms may tunnel into the deep layers at this step[39]. At the third step, position exchanges between the Pt atoms and O atoms would happen, which would greatly disorder the structure of the surface layers of Pt and weaken the interaction between the surface Pt layer (Pt^{2+} or PtO_x)
[40] and the bulk Pt metal, finally leading to the escape of surface Pt species into the solution. These dissolved Pt species then migrated to the cathode area and were regenerated on the Pt-GE by electrochemical or hydrogen reduction. As a result, the Pt-GE was activated gradually and exhibited high
[45] catalytic performance on HER.
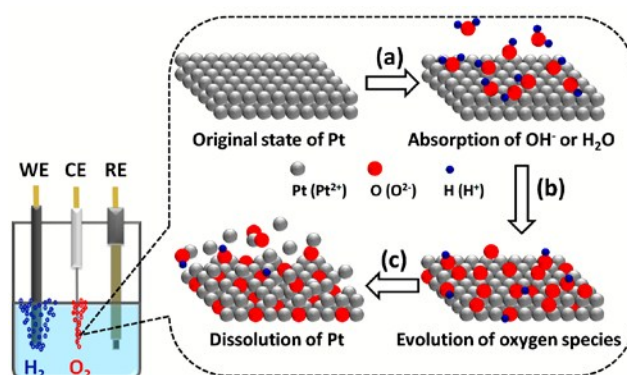
Fig.5 The possible schematic illustration for the transfer process of Pt from the anode to the cathode. (a) absorption of OH^- or H_2O on Pt surface, (b) evolution of oxygen species and their reaction with the Pt atoms, (c)
[50] position exchange between oxygen and Pt atoms and the dissolution of Pt.

3.6 Effect of CV cycling on carbon nanohorn catalyst

As discussed in the previous sessions, the activation of graphite rod may be ascribed to the deposition of Pt nanoparticles which was dissolved from the anode. However,
[55] the activation behaviour of nano-sized carbon might be possibly different. In this case, carbon nanohorns are a type of carbon nanomaterial with high surface area, good electrical conductivity and close to perfect chemical stability (ESI Fig S6). It can be produced in large-scale by DC arc
[60] discharge or laser ablation without any metal contamination. By purposely, CNHs were employed as a substitute to graphite rod and studied its activation process with the same procedure applied to Pt-GE and G-GE. Similar results to the ones of graphite rod were acquired and shown
[65] in Fig. 6. It is obvious that when a Pt wire was used as the counter electrode, CNHs was effectively activated after 4000 CV cycles; however, when a graphite rod was used as the counter electrode, CNHs was not activated successfully after 4000 CV cycles or even a potentiostatic treatment of 20000 s
[70] at -2.0 V. All these findings affirmed again that the use of Pt wire was necessary for the successful activation of carbon materials.
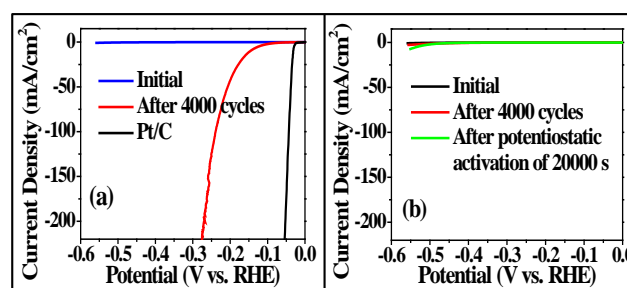
Fig.6 LSV curves of HER on CNH activated with Pt wire (a) and graphite
[75] rod (b) as counter electrodes. The HER curve on commercial Pt/C is also shown for comparison.

4. Conclusions

The activation of graphite rod was investigated when using different counter electrode during the CV cycling process.
[80] When a Pt wire used for activation, the electrochemical catalytic activity of graphite working electrode was greatly

improved to the extent as good as that on commercial Pt/C; but when a graphite rod was used, the working electrode couldn't be activated effectively. It was found that the formation of Pt nanoparticles on the cathode surface was the prime reason for the sharp increase in HER catalytic performance under activation with the Pt wire. However, further investigation is needed to determine how the Pt metal gets dissolved in the solution and regenerated onto the cathode for the formation of these Pt nanoparticles. At the same time, similar experiments were performed on the carbon nanohorns and found consistent results on the electrochemical catalysis for HER. It can be deduced that the use of Pt wire was essential for the successful activation of carbon materials. In any case, this work suggests that even though platinum is one of the most stable metals and widely used in electrochemical measurement as an inert electrode, its dissolution is ineligible in strongly acidic and low potential conditions, especially under the continuous CV scan. In some situations, the error caused by Pt dissolution may lead to inaccurate results and wrong conclusions. In order to completely exclude the disturbance from Pt dissolution, an inert counter electrode such as the graphite rod should be an ideal selection.

Acknowledgements

Notes and references

a Department of Physics and Materials Science, City University of Hong Kong, 83 Tat Chee Avenue, Kowloon Tong, Kowloon, Hong Kong. E-mail: johnnyho@cityu.edu.hk; saitchu@cityu.edu.hk
b Shenzhen Research Institute, City University of Hong Kong, Shenzhen, People's Republic of China
c State Key Laboratory of Silicon Materials, Key Laboratory of Advanced Materials and Applications for Batteries of Zhejiang Province, School of Materials Science and Engineering, Zhejiang University, Hangzhou, Zhejiang 310027, People's Republic of China.
d Department of Biology and Chemistry, City University of Hong Kong, 83 Tat Chee Avenue, Kowloon, Hong Kong
e Cultivation Base for State Key Laboratory, Qingdao University, No. 308 Ningxia Road, Qingdao, People's Republic of China

† Electronic Supplementary Information (ESI) available: [Experimental details of Pt/C powder and CNHs, the details about the EDS analysis of Pt wire and graphite rod, additional electrochemical data and TEM image of CHNs].
See DOI: 10.1039/b000000x/
‡ These authors contributed equally to this work.

References

1. J. D. Holladay, J. Hu, D. L. King and Y. Wang, *Catal Today*, 2009, 139, 244-260.
2. FuelCellToday, *The Industry Review 2013*, http://www.fuelcelltoday.com/.
3. A. Ursua, L. M. Gandia and P. Sanchis, *Proceedings of the IEEE*, 2012, 100, 410-426.
4. R. Subbaraman, D. Tripkovic, K.-C. Chang, D. Strmcnik, A. P. Paulikas, P. Hirunsit, M. Chan, J. Greeley, V. Stamenkovic and N. M. Markovic, *Nat Mater*, 2012, 11, 550-557.
5. C. G. Morales-Guio, L. A. Stern and X. L. Hu, *Chem Soc Rev*, 2014, 43, 6555-6569.
6. J. Kibsgaard, T. F. Jaramillo and F. Besenbacher, *Nat Chem*, 2014, 6, 248-253.
7. D. S. Kong, H. T. Wang, Z. Y. Lu and Y. Cui, *J Am Chem Soc*, 2014, 136, 4897-4900.
8. Z. Zhang, B. P. Lu, J. H. Hao, W. S. Yang and J. L. Tang, *Chem Commun*, 2014, 50, 11554-11557.
9. F. Jiao and H. Frei, *Energ Environ Sci*, 2010, 3, 1018-1027.
10. D. Merki and X. L. Hu, *Energ Environ Sci*, 2011, 4, 3878-3888.
11. J. Q. Zhuo, T. Y. Wang, G. Zhang, L. Liu, L. B. Gan and M. X. Li, *Angew Chem Int Edit*, 2013, 52, 10867-10870.
12. W. Cui, Q. Liu, N. Y. Cheng, A. M. Asiri and X. P. Sun, *Chem Commun*, 2014, 50, 9340-9342.
13. R. K. Das, Y. Wang, S. V. Vasilyeva, E. Donoghue, I. Pucher, G. Kamenov, H. P. Cheng and A. G. Rinzler, *Acs Nano*, 2014, 8, 8447-8456.
14. F. von Sturm, *Angewandte Chemie*, 1988, 100, 1260-1261.
15. W. J. Zhou, Y. C. Zhou, L. J. Yang, J. L. Huang, Y. T. Ke, K. Zhou, L. G. Li and S. W. Chen, *J Mater Chem A*, 2015, 3, 1915-1919.
16. Y. G. Li, H. L. Wang, L. M. Xie, Y. Y. Liang, G. S. Hong and H. J. Dai, *J Am Chem Soc*, 2011, 133, 7296-7299.
17. W. Sheng, Z. Zhuang, M. Gao, J. Zheng, J. G. Chen and Y. Yan, *Nat Commun*, 2015, 6. doi:10.1038/ncomms6848.
18. S. Iijima, M. Yudasaka, R. Yamada, S. Bandow, K. Suenaga, F. Kokai and K. Takahashi, *Chem Phys Lett*, 1999, 309, 165-170.
19. N. Li, Z. Y. Wang, K. K. Zhao, Z. J. Shi, Z. N. Gu and S. K. Xu, *Carbon*, 2010, 48, 1580-1585.
20. L. Shi, R. P. Liang and J. D. Qiu, *J Mater Chem*, 2012, 22, 17196-17203.
21. A. S. Arico, A. K. Shukla, H. Kim, S. Park, M. Min and V. Antonucci, *Appl Surf Sci*, 2001, 172, 33-40.
22. J. N. Tiwari, F. M. Pan, R. N. Tiwari and S. K. Nandi, *Chem Commun*, 2008, DOI: Doi 10.1039/B813935k, 6516-6518.
23. M. Hiramatsu and M. Hori, *Materials*, 2010, 3, 1559-1572.
24. M. Li, X. J. Bo, Z. C. Mu, Y. F. Zhang and L. P. Guo, *Sensor Actuat B-Chem*, 2014, 192, 261-268.
25. M. H. Huang, G. F. Dong, N. Wang, J. X. Xu and L. H. Guan, *Energ Environ Sci*, 2011, 4, 4513-4516.
26. J. S. Hammond and N. Winograd, *J Electroanal Chem*, 1977, 78, 55-69.
27. C. R. Parkinson, M. Walker and C. F. McConville, *Surf Sci*, 2003, 545, 19-33.
28. K. I. Ota, S. Nishigori and N. Kamiya, *J Electroanal Chem*, 1988, 257, 205-215.
29. G. Inzelt, B. B. Berkes and A. Kriston, *Pure Appl Chem*, 2011, 83, 269-279.
30. B. E. Conway, *Prog Surf Sci*, 1995, 49, 331-452.
31. H. S. Liu, C. J. Song, L. Zhang, J. J. Zhang, H. J. Wang and D. P. Wilkinson, *J Power Sources*, 2006, 155, 95-110.
32. A. A. Topalov, I. Katsounaros, M. Auinger, S. Cherevko, J. C. Meier, S. O. Klemm and K. J. J. Mayrhofer, *Angew Chem Int Edit*, 2012, 51, 12613-12615.
33. L. Kim, C. G. Chung, Y. W. Sung and J. S. Chung, *J Power Sources*, 2008, 183, 524-532.
34. S. Shrestha, Y. Liu and W. E. Mustain, *Catal Rev*, 2011, 53, 256-336.
35. R. Borup, J. Meyers, B. Pivovar, Y. S. Kim, R. Mukundan, N. Garland, D. Myers, M. Wilson, F. Garzon, D. Wood, P. Zelenay, K. More, K. Stroh, T. Zawodzinski, J. Boncella, J. E. McGrath, M. Inaba, K. Miyatake, M. Hori, K. Ota, Z. Ogumi, S. Miyata, A. Nishikata, Z. Siroma, Y. Uchimoto, K. Yasuda, K. I. Kimijima and N. Iwashita, *Chem Rev*, 2007, 107, 3904-3951.
36. S. Mitsushima, S. Kawahara, K. I. Ota and N. Kamiya, *J Electrochem Soc*, 2007, 154, B153-B158.
37. A. Kawano and S. Imabayashi, *J Electrochem Soc*, 2014, 161, F67-F71.

Journal of Materials Chemistry A Accepted Manuscript

38. S. Cherevko, A. A. Topalov, A. R. Zeradjanin, G. P. Keeley and K. J. J. Mayrhofer, *Electrocatalysis-Us*, 2014, 5, 235-240.
39. M. Matsumoto, T. Miyazaki and H. Imai, *J Phys Chem C*, 2011, 115, 11163-11169.
5   40. X. P. Wang, R. Kumar and D. J. Myers, *Electrochem Solid St*, 2006, 9, A225-A227.
41. Y. Sugawara, T. Okayasu, A. P. Yadav, A. Nishikata and T. Tsuru, *J Electrochem Soc*, 2012, 159, F779-F786.
42. H. Dau, C. Limberg, T. Reier, M. Risch, S. Roggan and P. Strasser,
10   *Chemcatchem*, 2010, 2, 724-761.

TOC (8x 4cm)
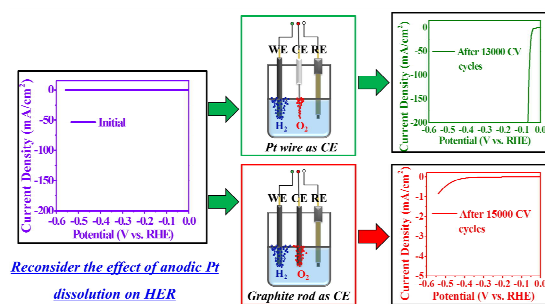
The anodic Pt dissolution, although being widely ignored, should be taken into reconsiderations during electrochemical tests when Pt metal is utilized as the counter electrode.